CORRELATION BETWEEN SEISMIC WAVE VELOCITY, ROCK POROSITY, AND MAXIMUM PRINCIPAL STRESS BASED ON THE LABORATORY TEST DATA

Chai Jinfei[1] – Wu Shunchuan[2,3*] – Tibbo Maria[4]

[1] Railway Engineering Research Institute, China Academy of Railway Sciences Corporation Limited, Beijing 100081, China
[2] Faculty of Land Resources Engineering，Kunming University of Science and Technology，Kunming，Yunnan 650093，China
[3] Key Laboratory of Ministry of Education for Efficient Mining and Safety of Metal Mine, School of Civil and Resource Engineering, University of Science and Technology Beijing 100083, China
[4] Department of Physics, University of Toronto, Toronto, Ontario, M5S 1A7, Canada

ARTICLE INFO

***Article history*:**
Received: 21.9.2016.
Received in revised form: 18.1.2017.
Accepted: 30.1.2017.

***Keywords*:**
Wave velocity
Axial pressure
Rock porosity
Crack density parameter
Rock specific

DOI: *http://doi.org/10.30765/er.39.1.5*

Abstract:

In order to determine the internal relationships among seismic wave velocity, axial pressure, and rock porosity, the rock samples taken from NRS170143 borehole of the Nickel Rim South mine are tested using a Hoek type triaxial cell equipped with axial linear variable differential transducers (LVDTs) and a data acquisition module. The empirical expression between seismic wave velocity and rock pressure is fitted based on the laboratory test data of rock samples. Then, P-V model P-φ model and φ-ε model are created to analyze the laboratory test data. The results show that: (1) the relationship between axial pressure and rock porosity can be represented by a new empirical equation $\varphi=a*e^{-b*P}-c$. *With an increase of axial pressure, the value of rock porosity gradually decreases below the straight line φ=1% and close to 0. The P-φ model can be a good judge if the pressure has reached the maximum compression pressure in the process of rock compression experiment; (2) The P wave velocity and S wave velocity exponentially increase with increasing axial pressure; Rock porosity and crack density parameter exponentially decrease with increasing axial pressure; (3) there is a linear positive correlation between the ratio of rock porosity to crack density parameter and the ratio of crack thickness to crack length. (4) the relationship between* V_p *and* V_s *in each compression test can be fitted to the linear equation* $V_p=a*V_s+b$; *for all different samples of NR170143, the ratios (M) of* V_p *to* V_s *ranges from 1.35 to 1.85. In summary, the P-V model, P-φ model, φ-ε model and* V_p-V_s-φ *model can intuitively reflect the relationship among seismic wave velocity, axial pressure and rock porosity.*

[*] Corresponding author. Tel.: +86-01051874086; fax: +86-01051874086
E-mail address: wushunchuan@163.com

1 Introduction

Rock mechanics parameters, seismic rock physics parameters, and rock porosity are very important rock properties in the field of geotechnical, mining and petroleum engineering. The bulk modulus (K), and shear modulus (μ), can be calculated from wave velocities [1-2]. The rock specific results have been obtained through related geophysical research [3-7].

There are many cracks distributed in natural rock because of forming conditions and changing environment. A multi-interrogation ultrasonic technique and correlation of several parameters such as attenuation, acoustic velocity and grain size with material features are covered in [8]. The properties of these cracked rocks are critically affected by the pressure (P) of the surrounding rocks. The constituent minerals and micro-cracks dictate the rock sample's response to stress. This behavior is reflected in the compressional and shear velocities measured in the laboratory as a function of confining pressure. Therefore, laboratory velocities have been employed to solve important geologic problems [8]. The nonlinear relationship of confining pressure (P) and seismic wave velocity (V) was first noticed by [9].

Rock porosity (φ) also significantly impacts on the elastic properties and seismic velocities of a material [11]. An in-depth analysis of void evolution and coalescence in simple shear was performed and revealed the complex relationship between the void shape and spacing on coalescence [12]. The correlations between uniaxial compressive strength and porosity using hornfelsic rocks collected from western Iran were analyzed in 1965 [13]. The expressions of modulus (bulk modulus and shear modulus) and porosity derived in 1950 using spherical pores in solids [14]. To overcome the limitations above, many researchers have developed two main kinds of methods: the Effective Matrix and the Effective Field [1,15]. Differential Effective Medium methods [16-17] and Self-Consistent methods [18] are two groups of Effective Matrix approaches. The Differential Effective Medium methods consider that pores are iteratively added to a matrix of solids. However, Self-Consistent methods consider the pores and solids as a whole. The Effective Field methods [19] create a stress field by injecting pores in the nonporous solid.

The change of rock porosity is often due to rock cracks. A lot of competing models are created to analyze the relationship between rock porosity and cracks [11]. The Self-Consistent method is extended to verify the importance of loading history [20]. The Mean Field method is used to explain the dynamic influences of both randomly oriented and aligned cracks, [21]. The Dislocation theory [22] is developed to solve the deformations connected with a closer to the real crack geometry with tapered edges.

The Self-Consistent method [18, 23] is widely used to explain the effect of porosity on rock properties through fitting the general form (flat circle form) of rock cracks using the quantified relationship between the micro-fracture source parameters.

Confining pressure has a great effect on rock elastic moduli in rocks with porosity φ<1% [9]. After theoretically testing a number of possible hypotheses, it was inferred that this nonlinear behavior must be due to the existence of crack-like pores of small aspect ratio.

However, the above methods are mainly used in the field of composite materials but are rarely applied in the fields of rock physics or geophysics [15]. In this paper the above-mentioned methods were applied to analyze the internal relationships among seismic wave velocity, axial pressure, and rock porosity.

2 Theory and methodology

In order to describe the relationship between pressure and seismic wave velocity in rocks, the following empirical expression has been summarized using a large number of experiments [10].

$$V = V_0 + D \cdot P - B \cdot e^{-k \cdot P} \tag{1}$$

where V is the wave velocity with some cracks: P wave velocity (V_P) or S wave velocity (V_S); P is the effective pressure applied to rock; V_0 is the wave velocity without crack: P wave velocity (V_{P0}) or S wave velocity (V_{S0}); and B, D, and k are fitting parameters. D is often left as zero as it can result in unreasonable values at elevated pressures [17].

The bulk modulus (K), and the shear modulus (μ), can be calculated from P and S wave velocities [2].

$$K = \rho\left(V_P^2 - \frac{4V_S^2}{3}\right) \tag{2}$$

$$\mu = \rho V_S^2 \tag{3}$$

According to Mackenzie's expressions [4] for the case of cracked rock, the relationship between bulk modulus (K_d) and porosity (φ) takes the form

$$K_d = \frac{K_m}{1+\frac{3\varphi(1-\sigma_m)}{2(1-\varphi)(1-2\sigma_m)}} \quad (4)$$

And the relationship between shear modulus μ_d and porosity (φ) takes the form

$$\mu_d = \frac{\mu_m(1-\varphi)}{1+\frac{\varphi(12+6K_m/\mu_m)}{(8+9K_m/\mu_m)}} \quad (5)$$

So, the rock porosity can be calculated from

$$\varphi = \frac{1}{1+\frac{3(1-\sigma_m)}{2(K_m/K_d-1)(1-2\sigma_m)}} \quad (6)$$

According to Self-Consistent forms [23], the effective Poisson's ratio of the cracked solid σ_d can first be found from

$$\sigma_d = \frac{1}{2}\left(\frac{V_P^2-2V_S^2}{V_P^2-V_S^2}\right) \quad (7)$$

If the crack length (a) is equal to the crack width (b), the crack density parameter equation is given by article [23].

$$\varepsilon = N\langle a^3\rangle \quad (8)$$

The relationship of bulk modulus K_d and crack density parameter ε is given by [23].

$$K_d = K_m\left(1-\frac{16(1-\sigma_d^2)}{9(1-2\sigma_d)}\varepsilon\right) \quad (9)$$

So, the crack density parameter can be calculated by

$$\varepsilon = \frac{9\left(1-\frac{K_d}{K_m}\right)(1-2\sigma_d)}{16(1-\sigma_d^2)} \quad (10)$$

According to article [18] and [23], the crack porosity can be described as by equation (11).

$$\varphi = \frac{4N\pi}{3}\langle a^2c\rangle \quad (11)$$

where: c is the thickness of the crack.
Incorporating equation (8) and equation (11), the relationship between the crack parameter and porosity is given by equation (12).

$$\varepsilon = \frac{3a}{4\pi c}\varphi = \frac{3}{4\pi\alpha}\varphi \quad (12)$$

Where $\alpha=c/a$.

3 Geology and laboratory test

Approximately 2 billion years ago, a meteorite crashed into earth at what is now Sudbury, Ontario, Canada. The collision was so violent that it liquefied the metals in the earth's surface. These metals settled on the rim of the crater and on the crater's outside wall creating the Sudbury Basin, a 100 km (62 mile) wide, 15 km (9 mile) deep, oval shaped deposit that is one of the richest nickel deposits in the world. Discovered in 2001 and under construction since March 2004, Nickel Rim South boasts an 18.2 million tons resource distributed almost equally between two adjacent ore bodies: a copper and precious metal-rich footwall zone with copper grades averaging 7% and a contact zone grading 2% nickel [24].
A 3D schematic of the ore distribution and exploitation works for the Copper/ Nickel Deposit at Nickel Rim South mine is shown in Fig. 1.
115 rock samples from different depths along borehole NR170143 (Table 1), were tested. Sample dimensions were reduced to Height=170mm, Radius=50.8mm and tested in the laboratory to analyze the relationship between hard rock porosity and other parameters (as shown in Table 1). The test facilities at the Lassonde Institute of Mining, University of Toronto were used and a Hoek type triaxial cell with axial linear variable differential transformers (LVDTs) and data acquisition module (as shown in Fig. 2) was employed for this testing.

Table 1. Geophysical properties of drill core from NRS170143

Lithology	Sample Number	Depth along Borehole (m)	Geology	Density (g/cm^3)	Photos of Samples
Norite	16	59.54	FNOR	2.780	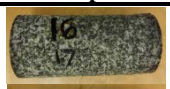
	34	129.98	FNOR	2.820	
	40	154.00	DNOR	3.080	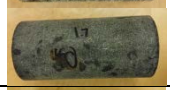
Breccia	43	165.58	LGBX	2.890	
	69	259.92	SDBX	2.820	
	108	374.04	SDBX	3.030	
Gneiss	77	276.00	FGN	2.640	
	85	291.80	FGN	2.640	
Tonalite or Granodiorite	95	321.98	TON	2.780	
	50	194.11	GRDR	2.890	

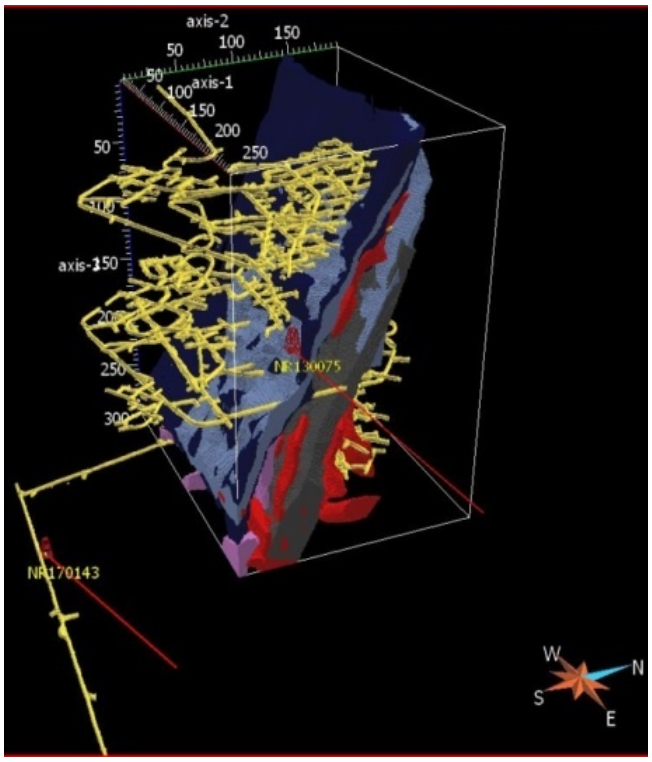

Figure 1. Copper / Nickel Deposit.

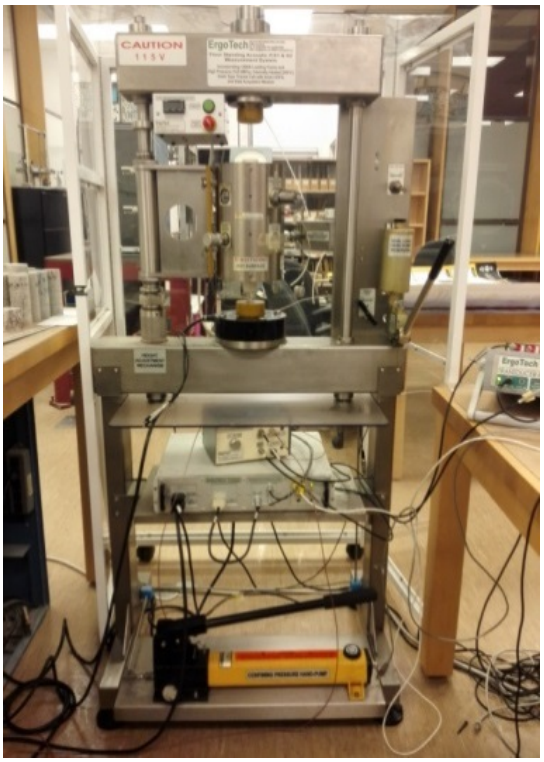

Figure 2. Hoek type triaxial cell.

4 The results and discussion

This paper analyzed the laboratory test data of the Sample No.16 No.34 No.85 No.95, No.108 for example from 115 samples of NRS170143.

According to the fitted relationships of loading test and unloading test data between axial pressure and seismic wave velocity, the *B* values of the fitted relationship, equation (1), in unloading compression test is generally larger than the *B* values in loading compression test using the same sample. This phenomenon is due to closed pores because of loading compression failed to reopen to the original stress state.

Under the original stress state, the rule of loading compression test data is not obvious due to the cracks in the rock samples being very complex, such as uneven distribution or irregular form of crack; but the rules of unloading recovery test data are more obvious. Therefore, this paper uses the unloading recovery test data to analyze the correlation between each parameter.

The relationship between axial pressure and seismic wave velocity (*V*) has been summed up into equation (1) by many scientists. Using the uniaxial compression test unloading data of Sample No.16, No.34, No.85 and No.95, the relationship (equation 13-20) between axial pressure and seismic wave velocity can be created in *P*-V_p model and *P*-V_s model.

Along the fitted lines (blue lines and red lines) in Fig. 3 (a), (c), (e), (g), the seismic wave velocity (V_p, V_s) increases with increasing axial pressure of uniaxial compression test.

$$V_{p\_16}=6.043-0.8303*e^{-0.06274*P} \quad (13)$$
$$V_{s\_16}=3.568-0.4633*e^{-0.04079*P} \quad (14)$$
$$V_{p\_34}=6.090-0.9290*e^{-0.04230*P} \quad (15)$$
$$V_{s\_34}=3.550-0.5505*e^{-0.03395*P} \quad (16)$$
$$V_{p\_85}=6.071-1.0180*e^{-0.03013*P} \quad (17)$$
$$V_{s\_85}=3.493-0.4734*e^{-0.04077*P} \quad (18)$$
$$V_{p\_95}=6.506-1.0440*e^{-0.02204*P} \quad (19)$$
$$V_{s\_95}=3.642-0.4154*e^{-0.02993*P} \quad (20)$$

In the next step, the relationship between axial pressure and rock porosity need to be investigated using the test data for Samples No.16, No.34, No.85, No.95, since this relationship has not been clearly established.

Rock porosities of these samples can be obtained by equation (6). The dots of axial pressure and rock porosity can be plotted in Fig. 3 (b), (d), (f), (h). The fitted relationships between axial pressure data and rock porosity data are shown in equations (21-24). By summarizing these equations, an empirical equation about the relationship of axial pressure and porosity can be summed up as equation (25).

The rock porosity value of Sample No.16, No.34, No.85, No.95 gradually decreases under the straight line φ=1% and close to 0 with the increase of axial pressure.

$$\varphi=0.01650*e^{-0.07843*P}+0.000754 \quad (21)$$
$$\varphi=0.01513*e^{-0.05223*P}+0.01524 \quad (22)$$
$$\varphi=0.02069*e^{-0.002627*P}-0.02828 \quad (23)$$
$$\varphi=0.01910*e^{-0.02103*P}+0.03518 \quad (24)$$
$$\varphi=a*e^{-b*P}-c \quad (25)$$

To test and verify the adaptability of *P*-*V* model and *P*-φ empirical equation in other samples, the uniaxial and triaxial compression test data of Sample No.108 are analyzed as follows.

Using the same method, the *P*-V_p model and the *P*-V_s model of Sample No.108 can be created as shown in Fig. 4 (a), (b). Four limiting lines (equations 26-29) can be created in *P*-V_p model and *P*-V_s model. Almost all data are located in the area between the limiting lines. Using the *P*-*V* model, the range of seismic wave velocities can be computed from the rock axial pressure, and vice versa.

$$V_{p\_up}=6.41-0.1854*e^{-0.02716*P} \quad (26)$$
$$V_{p\_down}=6.40-0.3006*e^{-0.01589*P} \quad (27)$$
$$V_{s\_up}=3.70-0.1058*e^{-0.06413*P} \quad (28)$$
$$V_{s\_down}=3.69-0.2070*e^{-0.03343*P} \quad (29)$$

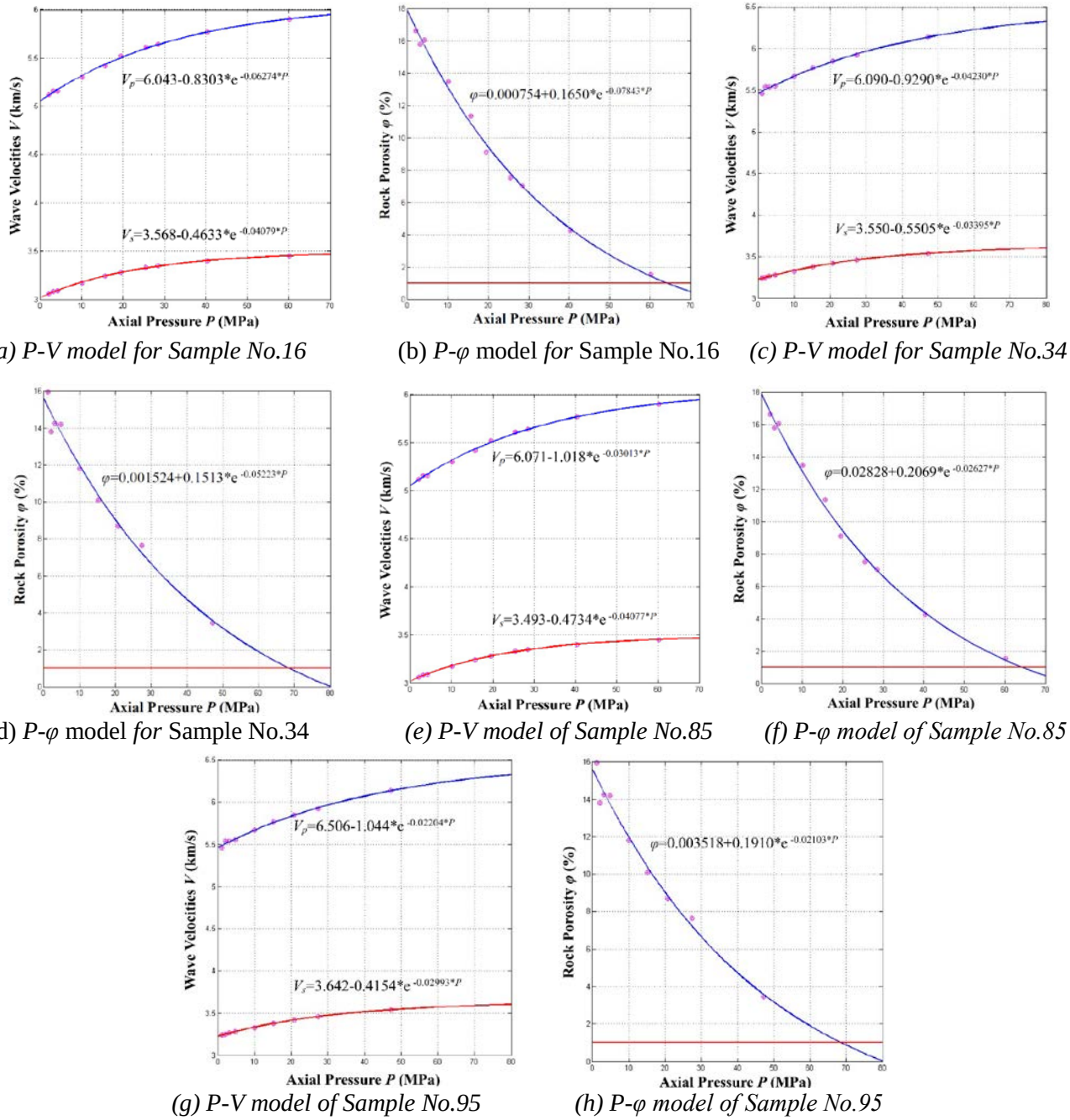

(a) P-V model for Sample No.16 (b) *P-φ* model *for* Sample No.16 *(c) P-V model for Sample No.34*

(d) *P-φ* model *for* Sample No.34 *(e) P-V model of Sample No.85* *(f) P-φ model of Sample No.85*

(g) P-V model of Sample No.95 *(h) P-φ model of Sample No.95*

Figure 3. The P-V_p model and the P-φ model for Sample No.16, No.34, No.85, No.95 using laboratory test data. Magenta dots are laboratory test data. Blue lines are fitted lines of laboratory test data. Red lines are the line φ=1%.

Rock porosities of samples can be obtained by equations (2) and (6). The dots of axial pressure and rock porosity can be plotted in Fig 4 (c). And the fitted relationships of loading compression test and unloading recovery test data between axial pressure and rock porosity are shown in equations (30)-(37) which are all fitted to equation (25).

$$\varphi=0.02669*e^{-0.04554*P}+0.01221 \quad (30)$$
$$\varphi=0.02330*e^{-0.08588*P}+0.01226 \quad (31)$$
$$\varphi=0.06276*e^{-0.003052*P}-0.03437 \quad (32)$$
$$\varphi=0.02223*e^{-0.04324*P}+0.01233 \quad (33)$$
$$\varphi=0.06962*e^{-0.003091*P}-0.04070 \quad (34)$$
$$\varphi=0.02253*e^{-0.02264*P}+0.01037 \quad (35)$$
$$\varphi=0.04308*e^{-0.01002*P}-0.01064 \quad (36)$$
$$\varphi=0.05013*e^{-0.006971*P}-0.01814 \quad (37)$$

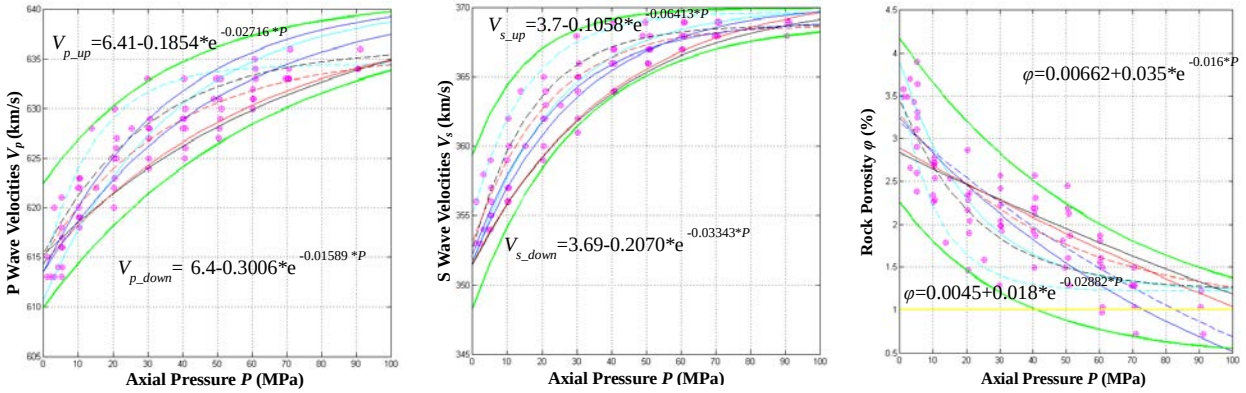

(a) P-V_p model of Sample No.108 *(b) P-V_s model for Sample No.108* *(c) P-φ model for Sample No.108*

Figure 4. P-Vp model, P-Vp model and P- ϕ model using the laboratory test data of Sample No.108. Magenta dots are laboratory test data. Blue lines are fitted lines of laboratory tests with different radial pressure. Solid lines are fitted lines of loading data; Dotted lines are fitted lines of unloading data. Cyan lines are fitted lines of uniaxial compression test data. Black lines are fitted lines of triaxial compression test data with Axial Pressure/Radial Pressure=1.6. Red lines are fitted lines of triaxial compression test data with Axial Pressure/Radial Pressure=1.3. Blue lines are fitted lines of triaxial compression test data with Axial Pressure/Radial Pressure=1. Green lines are limit lines of laboratory test data. Yellow lines are the line 1%.

Using equation (25), 2 limiting lines (equation 38-39) can be drawn in the *P*-φ model. Almost all data are located in the area between the 2 limiting lines as shown in Fig. 4 (c). Using the *P*-φ model, the range of rock porosity can be computed from rock axial pressure, and vice versa. As in the case of the rock porosities for Sample No.16, No.34, No.85, No.95, the rock porosities for Sample No.108 also gradually decrease under the straight line φ=1% and close to 0 with the increase of axial pressure.

$$\varphi=0.03500*e^{-0.01600*P}+0.00662 \quad (38)$$

$$\varphi=0.01800*e^{-0.02882*P}+0.00450 \quad (39)$$

According to equation (10), the rock crack density parameter (ε) can be computed from the bulk modulus (K) using laboratory test data of sample No.108. The relationship between rock porosity (φ) data and crack density parameter (ε) data fits equation (40) as follows.

As shown in equation (40), the ratio (α) of crack thickness (c) to crack length (a) can be computed from the equation (41). Using the φ-ε model (equation (40)), mutual conversion between rock porosity (φ) and crack density parameter (ε) can be achieved. Along the fitted line in Fig. 5, crack density parameter increases with increasing rock porosity.

$$\varepsilon=\frac{3a}{4\pi c}\varphi=\frac{3}{4\pi\alpha}\varphi=0.6574\varphi \quad (40)$$

$$\alpha=\frac{c}{a}=0.3631 \quad (41)$$

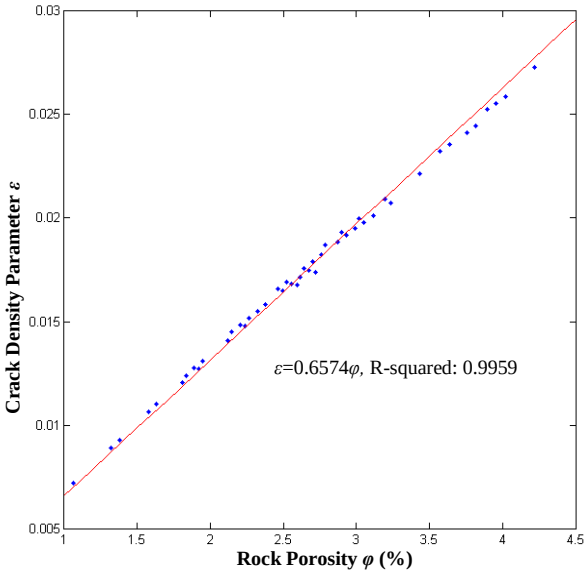

Figure 5. φ-ε model for sample No.108. Blue dots are computed from laboratory test data. Red line is fitted line.

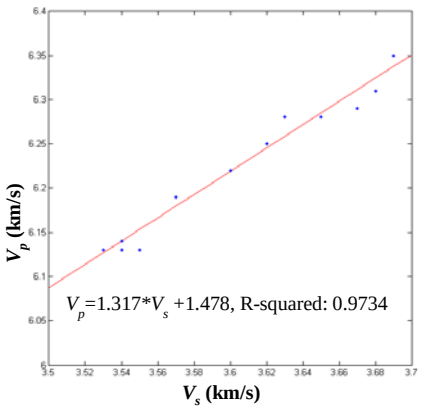

(a) Uniaxial loading test data for Sample No.108

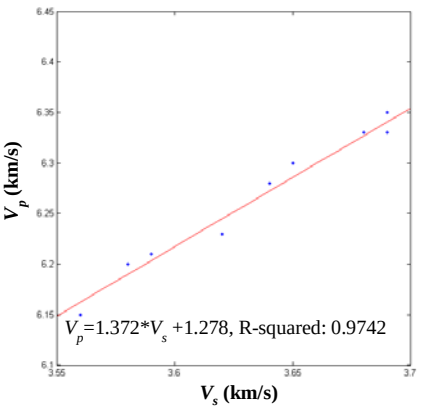

(b) Uniaxial unloading test data for Sample No.108

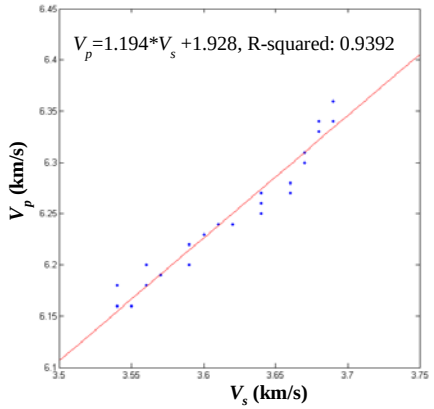

(c) Triaxial loading test data for Sample No.108

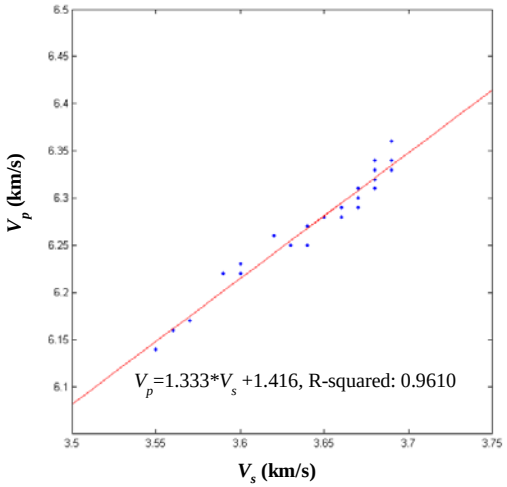

(d) Triaxial unloading test data for Sample No.108

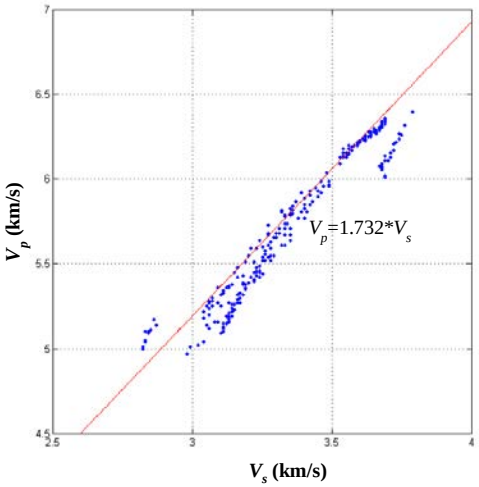

(e) All test data for all samples

Figure 6. Relationship between P wave velocity (V_p) and S wave velocity (V_s).

According to uniaxial compression test data (loading, unloading) and triaxial compression test data (loading, unloading) of sample No.108, the relationships between V_p and V_s of each compression test can be fitted to linear equations as shown in equations (42-45).

Then a general relationship between V_p and V_s of rock compression test can be summed up as the form of equation (46), which is named V_p-V_s model. The form of equation (46) is similar to the research of article [25], article [26] and article [27].

In V_p-V_s model of sample No.108, V_p increases with increasing V_s of uniaxial compression test and triaxial compression test. Using V_p-V_s model, mutual conversion between V_p and V_s can be achieved.

But if all laboratory test data of all different samples are shown in one diagram (Fig. 6 (e)), the relationships between V_p and V_s of all different samples are agreement with the form of expression as equation (47). It means that the Poisson's Ratio values of all different samples ranges from 2.4 to 2.6 computed by equation (7).

$$V_p=1.317*V_s+1.478 \quad (42)$$
$$V_p=1.372*V_s+1.278 \quad (43)$$
$$V_p=1.194*V_s+1.928 \quad (44)$$
$$V_p=1.333*V_s+1.416 \quad (45)$$
$$V_p=a*V_s+b \quad (46)$$
$$V_p=1.732*V_s \quad (47)$$

Based on the research of previous sections, a 3-parameters model (color line, equation (48)) of V_p and V_s and rock porosity (φ) using all uniaxial and triaxial test data of sample No.108 can be created by adding rock porosity (φ) parameter as shown in Fig. 7. In V_p-V_s-φ model of sample No.108, the value of

rock porosity (φ) is correlated with the value of V_p and V_s which are measured in uniaxial compression test and triaxial compression test. The value of V_p and V_s decreases with increasing value of rock porosity (φ).

$$V_p=1.282*V_s+1.607 \quad (48)$$

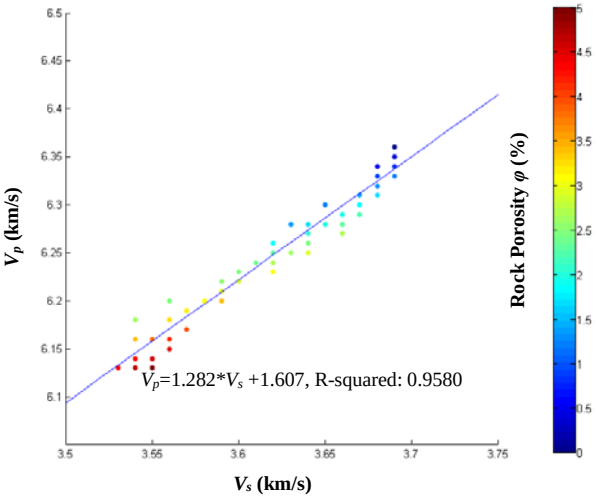

Figure 7. Relationship between P wave velocity (V_p), S wave velocity (V_s) and rock porosity (φ).

5 Conclusion

In this study, *P-V* model, *P-φ* model, and *φ-ε* model have been created to analyze the relationship among seismic wave velocity, axial pressure, and rock porosity using Sample No.16, No.34, No.85, No.95 and No.108 from NR170143 borehole of Copper/ Nickel Deposit of Nickel Rim South Mine in Sudbury.

The major conclusions of this work are:

(1) the relationship between axial pressure and rock porosity can be sum up into the empirical equation: $\varphi=a*e^{-b*P}-c$. Rock porosity has gradually decreased below the straight line φ=1% and close to 0 with the increase of axial pressure. The *P-φ* model can be a good judge whether the pressure has reached the maximum compression pressure in the process of rock compression experiment;

(2) when axial pressure (P) increases gradually, the seismic wave velocity (V_p, V_s) will also increase step by step in the test of uniaxial compression and triaxial compression; on the contrary rock porosity (φ) and crack density parameter (ε) will eventually decrease to 0;

(3) There is a linear positive correlation between the ratio of rock porosity (φ) and crack density parameter (ε) and the ratio (α) of crack thickness (c) to crack length (a);

(4) The relationship between V_p and V_s in each compression test can be fitted to the linear equation: $V_p=a*V_s+b$; for all different samples of NR170143, the ratios (M) of V_p to V_s ranges from 1.35 to 1.85;

In summary, *P-V* model, *P-φ* model, *φ-ε* model and V_p-V_s-φ model can intuitively reflect the relationship among seismic wave velocity, axial pressure and rock porosity.

Acknowledgements

The authors would like to thank the SUMIT program and the Fund project of China Academy of Railway Sciences (2017YJ050) for providing funding support; thanks to Professor Bernd Milkereit from University of Toronto for providing a lot of advice; thanks to the anonymous reviewers and the associate editor, whose constructive comments helped improve the presentation of this work.

References

[1] Mavko G, Mukerji T, Dvorkin J: *The rock physics handbook: tools for seismic analysis in porous media*, New York, Cambridge University Press, 2003.

[2] Birch F: *The velocity of compressional waves in rocks to 10 kilobars, part 2*, Journal of Geophysical Research, 1961, 66: 2199-2224.

[3] Milkereit B, Eaton D, Wu J, et al: *Seismic imaging of massive sulfide deposits, Part II*, Reflection seismic profiling. Economic Geology, 1996, 91(5): 829-834.

[4] Milkereit B, Berrer E K, Watts A, et al: *Development of 3-D seismic exploration technology for Ni-Cu deposits*, Sudbury Basin, Proceedings of Exploration, 1997, 97: 439-448.

[5] Milkereit B, Eaton D: *Imaging and interpreting the shallow crystalline crust*, Tectonophysics, 1998, 286(1): 5-18.

[6] Milkereit B, Berrer E K, King A R, et al: *Development of 3-D seismic exploration technology for deep nickel-copper deposits-A case history from the Sudbury basin*, Canada. Geophysics, 2000, 65(6): 1890-1899.

[7] Eaton D W, Milkereit B, Adam E: *3-D seismic exploration*, Proceedings of Exploration, 1997, 97: 65-78.

[8] Khaira A, Srivastava S, Suhane A: *Analysis of relation between ultrasonic testing and microstructure: a step towards highly reliable fault detection*, Engineering Review, 2015, 35(2): 87-96.
[9] Wepfer W W, Christensen N I: *A seismic velocity-confining pressure relation, with applications*, International Journal of Rock Mechanics and Mining Sciences & Geomechanics Abstracts, Pergamo, 1991, 28(5): 451-456.
[10] Adams L H, Williamson E D: *The compressibility of minerals and rocks at high pressures*, Journal of the Franklin Institute, 1923, 195: 475-529.
[11] Zimmerman R W, Somerton W, King M: *Compressibility of porous rocks*, Journal of Geophysical Research, 1986, 91: 12765-12777.
[12] Schmitt D. R.: *Geophysical properties of the near surface earth: seismic properties*, Treatise on Geophysics, 2nd edition, Oxford: Elsevier, 2015, 11:43-87.
[13] Rahman M A, Butcher C, Chen Z: *Void evolution and coalescence in porous ductile materials in simple shear*, International Journal of Fracture, 2012, 177(2): 129-139.
[14] Fereidooni D: *Determination of the geotechnical characteristics of hornfelsic rocks with a particular emphasis on the correlation between physical and mechanical properties*, Rock Mechanics and Rock Engineering, 2016, 49(7): 2595-2608.
[15] Mackenzie, J K: *The elastic constants of a solid containing spherical holes*, Proceedings of the Physical Society, Section B, 1950, 63: 2-11.
[16] Carvalho F C S, Labuz J F: *Experiments on effective elastic modulus of two dimensional solids with cracks and holes*, International Journal of Solids and Structures, 1996, 33: 4119-4130.
[17] David E C, Zimmerman R W: *Elastic moduli of solids containing spheroidal pores*, *International Journal of Engineering Science*, 2011, 49: 544-560.
[18] Zimmerman R W: *Elastic-moduli of a solid with spherical pores - New self-consistent method*, International Journal of Rock Mechanics and Mining Sciences, 1984, 21: 339-343.
[19] Budiansky B, O'Connell R J: *Elastic-moduli of a cracked solid*, International Journal of Solids and Structures, 1976, 12: 81-97.
[20] Mori T, Tanaka K: *Average stress in matrix and average elastic energy of materials with misfitting inclusions*, Acta Metallurgica, 1973, 21: 571-574.
[21] Horii H, Nemat-Nasser S: *Overall moduli of solids with microcracks: load-induced anisotropy*, Journal of the Mechanics and Physics of Solids, 1983 31(2): 155-171.
[22] Hudson J A: *Wave speeds and attenuation of elastic waves in material containing cracks*, *Geophysical Journal International*, 1981, 64(1): 133-150.
[23] Mavko G M, Nur A: *The effect of non-elliptical cracks on the compressibility of rocks*, Journal of Geophysical Research: Solid Earth, 1978, 83(B9): 4459-4468.
[24] O'Connell R J, Budiansky B: *Seismic velocities in dry and saturated cracked solids*, Journal of Geophysical Research, 1974, 79: 5412-5426.
[25] Gleason W: *Xstrata's Nickel Rim South project to join the prolific Sudbury Basin*, Canadian Mining: Mining Engineering, 2008, 8:24-28.
[26] Castagna J P, Batzle M L, Eastwood R L: *Relationships between compressional-wave and shear-wave velocities in clastic silicate rocks*, Geophysics, 1985, 50(4): 571-581.
[27] Castagna J P, Backus M M: *AVO analysis-Tutorial and review*, Offset-dependent reflectivity-Theory and practice of AVO analysis: SEG Investigations in Geophysics, 1993, 8: 3-36.
[28] Pickett G R: *Acoustic character logs and their applications in formation evaluation*, Journal of Petroleum technology, 1963, 15(6): 659-667.